J Solid State Electrochem (2009) 13:1387–1394
DOI 10.1007/s10008-008-0701-5

ORIGINAL PAPER

Influence of addition of cobalt oxide on microstructure and electrochemical capacitive performance of nickel oxide

Jing-Jing Deng · Jian-Cheng Deng · Zi-Ling Liu · Hui-Ren Deng · Bo Liu

Received: 3 September 2008 / Revised: 25 September 2008 / Accepted: 6 October 2008 / Published online: 21 October 2008

Abstract Ni–Co oxide nanocomposite was prepared by thermal decomposition of the precursor obtained via a new method—coordination homogeneous coprecipitation method. The synthesized sample was characterized physically by X-ray diffraction, scanning electron microcopy, energy dispersive spectrum, transmission electron microscope, and Brunauer–Emmett–Teller surface area measurement, respectively. Electrochemical characterization of Ni–Co oxide electrode was examined by cyclic voltammetry, galvanostatic charge–discharge, and electrochemical impedance measurements in 6-mol L^{-1} KOH aqueous solution electrolyte. The results indicated that the addition of cobalt oxide not only changed the morphology of NiO but also enhance its electrochemical capacitance value. A specific capacitance value of 306 F g^{-1} of Ni–Co oxide nanocomposite with n_{Co}=0.5 (n_{Co} is the mole fraction of Co with respect to the sum of Co and Ni) was measured at the current density of 0.2 A g^{-1}, nearly 1.5 times greater than that of pure NiO electrode. Lower resistance and better rate capability can also be observed.

Keywords Nickel–cobalt oxides · Coordination homogeneous coprecipitation method · Electrochemical capacitors · Composite materials

Introduction

Electrochemical capacitors, also called supercapacitors, attract growing attention due to the unique characteristic of the high power density, the excellent reversibility, and the longer cyclic life in comparison with batteries. These devices have applications in hybrid electric vehicles, computer power backup, power electronics, and space flight technology [1].

Transition metal oxides have been one of the most widely used active electrode materials [2–4]. Noble metal oxide such as RuO_2 has been identified as possibly the best electrode material for pseudocapacitors, with capacitance reported to be as large as 768 F g^{-1} [5]. But the high cost and scarce source of these materials retarded their commercial application. In this regard, the search for cheaper alternatives with sufficient pseudocapacitive performance is a very import issue. The natural abundance and low cost of nickel oxide, accompanied by its energy storage performance in basic electrolytes and environmental compatibility, have made it one of the most promising electrode materials for pseudocapacitors. Presently, several researchers have begun to develop various effective processes for producing NiO electrodes with pseudocapacitive properties. These methods include sol–gel method [6, 7], electrochemical route [8, 9], and chemical precipitation method [10, 11]. The morphology and doping technique were found to have obvious effect on specific capacitance of NiO electrode [11–13]. In fact, Co doping has been found to significantly enhance the redox reversibility of both Ni oxide [14, 15] and metal hydride [16] electrodes in the Ni–MH battery. However, only a few researchers reported the capacitive properties of binary Ni–Co oxides. Hu and Cheng [17] prepared hydrous nickel–cobalt oxides on graphite substrate by electrochemical anodic deposition method. However, the condition of this method was rigid, hard to realize the scale production, and the authors did not provide any information about the effect of addition of cobalt on the microstructure and capacitance of NiO.

J.-J. Deng · J.-C. Deng (✉) · Z.-L. Liu · H.-R. Deng · B. Liu
Key Laboratory of Environmentally Friendly Chemistry and Applications of Ministry of Education, College of Chemistry, Xiangtan University,
Xiangtan 411105 Hunan, China
e-mail: djcwye@163.com

In this paper, Ni–Co oxide nanocomposites were synthesized using nickelous carbonate and basic cobaltous carbonate as metal source, ammonia as coordination agent via coordination homogeneous coprecipitation method. During the synthesis process, anion that could not be easily removed was not introduced into reactant solution, so washing step was not needed, which cannot only predigest the production process and reduce the cost but also avoid the agglomeration of products resulted from washing processing. The method is simple, easy to realize the scale production.

Experimental

Synthesis of Ni–Co oxide nanocomposite

The mechanism of coordination homogeneous coprecipitation method is as follows: Firstly, two kinds of metal salts, nickelous carbonate and basic cobaltous carbonate, react with ammonia, forming a mixed complex solution ($[Ni(NH_3)_6]^{2+}$ and $[Co(NH_3)_6]^{2+}$) coexisting with precipitator (CO_3^{2-}). Subsequently, the mixture solution dissociates to release the metal ions by diluting the complex solution with distilled water and heating to remove ammonia from aqueous solution. As the ammonia concentration in the solution decrease and the free nickel and cobalt ions increase, when the metal cations and precipitator anions reach a certain amount, precipitates of basic nickel carbonate and basic cobalt carbonate mixed precursors are yielded homogeneously in the solution. Because the metal ions and precipitator are dispersed in the solution homogeneously, thus, the precipitation reaction can reach molecular level, which ensures the sedimentation yielding and separating out homogeneously from the solution. The reaction system did not introduce any other metal cation and anion that was uneasily removed, the very pure Ni–Co oxide nanocomposite powder could be obtained without washing process which usually results in the agglomeration of products, but just through centrifuging, desiccation, and calcination.

All the chemical reagents used in this experiment were analytical grade and used without further purification. Nickelous carbonate and basic cobaltous carbonate in a desired molar ratio (the total quantity was 0.02 mol) were dispersed in 20 ml distilled water, and then the dispersion was ultrasonically treated for 10 min. Then, a certain amount of concentrated ammonia (28 wt.%) was added into the suspension, forming a transparent mixed complex solution $[Ni(NH_3)_6]^{2+}$ and $[Co(NH_3)_6]^{2+}$. Then, the mixed solution was added into seven times volume distilled water and the reaction was carried out under magnetic string at 70 °C for 1 h. The precipitated precursors were separated by centrifugation and dried in a vacuum at 60 °C for 12 h. The final black powders were obtained by calcination in air at 350 °C for 2 h. By this way, we prepared Ni–Co oxide nanocomposites with n_{Co}=0, 0.2, 0.5, and 0.6, respectively (n_{Co} is the mole fraction of Co with respect to the sum of Co and Ni). These products were denoted as sample A, B, C, and D.

Characterization

Powder X-ray diffraction (XRD) measurements were carried out using a SIEMENS D-5000 automatic X-ray diffractometer (Cu Kα radiation λ=0.154178 nm, graphite monochromator, proportional counter). The surface morphology of products was obtained with HITHACH-4300 scanning electron microscope (SEM) instrument (Japan Electronic Company, Japan). A (HITACHI)-600 transmission electron microscope (TEM) was used to characterize the morphology and size of the products. The surface area was calculated using the Brunauer–Emmett–Teller (BET) equation. Pore size distributions were calculated by the Barrett–Joyner–Halenda method using the desorption branch of the isotherm.

Electrodes preparation and electrochemical tests

Electrodes for electrochemical capacitors were prepared by mixing the active materials with 20 wt.% acetylene black and 5 wt.% polytetrafluoroethylene of the total electrode mass. A small amount of alcohol was then added to this composite to make a more homogeneous mixture, which was pressed on nickel foam to fabricate the electrodes. Electrochemical behaviors were characterized by cyclic voltammetry, galvanostatic charge–discharge, and electrochemical impedance spectroscopy tests. The experiments were carried out in a three-electrode glass cell. The prepared electrode, nickel foam sheet, and saturated calomel electrode (SCE) were used as the working, counter, and reference electrodes, respectively. All the electrochemical measurements were performed in an electrolyte of 6.0-mol L^{-1} KOH solution and using a CHI660A electrochemical working station controlled by a computer.

Results and discussion

Formation of Ni–Co oxide

The XRD patterns of sample A (n_{Co}=0) and C (n_{Co}=0.5) are shown in Fig. 1a,b. In Fig. 1a, all these diffraction peaks, including not only the peak positions but also their relative intensities, can be perfectly indexed into the cubic crystalline structure of NiO. The result is in accordance with the standard spectrum (JCPDS, no. 47-1049). The corresponding results in Fig. 1b demonstrate that the nickel

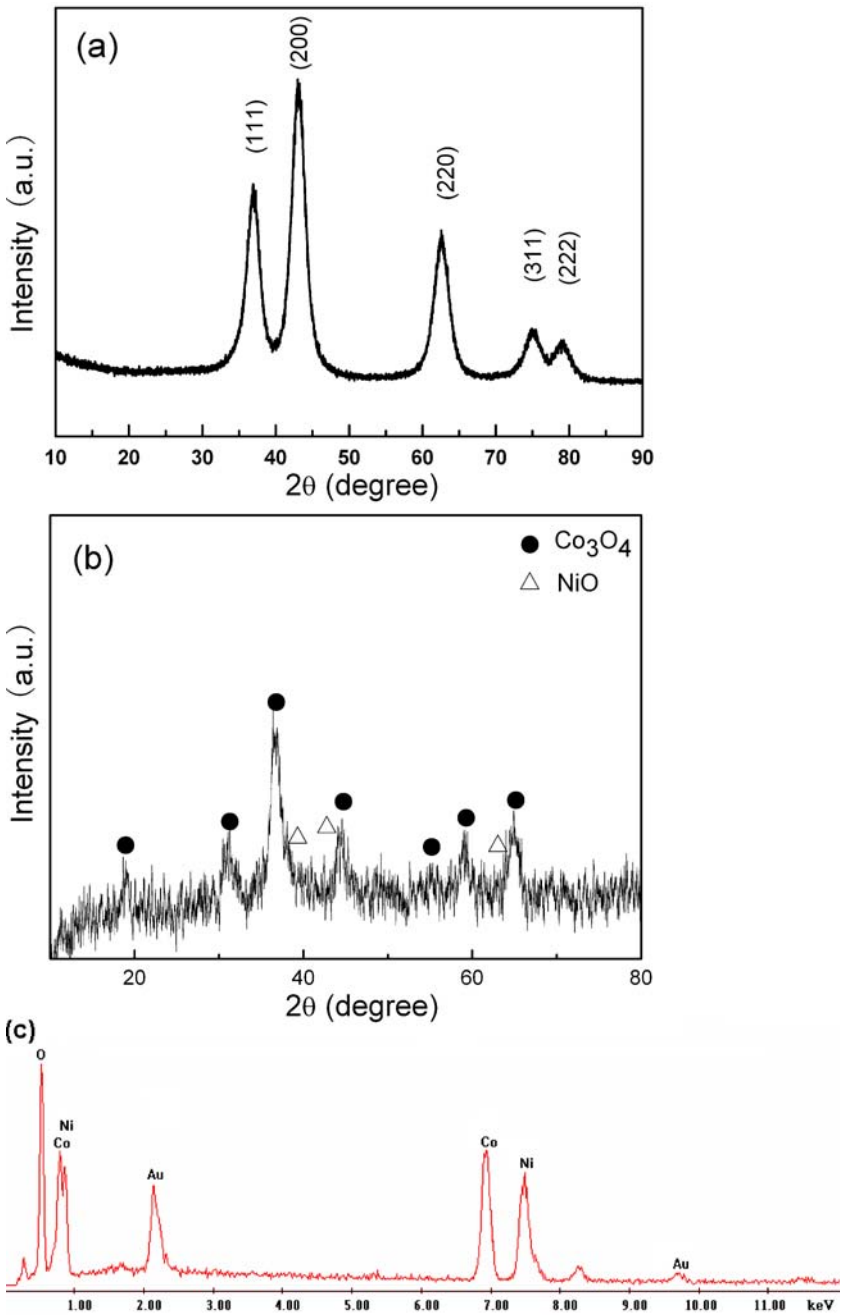

Fig. 1 **a** XRD pattern of sample A (n_{Co}=0); **b** XRD pattern of sample C (n_{Co}=0.5); **c** EDS analysis of sample C (n_{Co}=0.5)

and cobalt oxides in the composite exist as NiO (JCPDS, no. 47-1049) and Co_3O_4 (JCPDS, no. 73-1701), respectively. It is difficult to differentiate between the two phases, since they have similar structures, and their diffraction peaks are very close. The peaks in Fig. 1b are broad, which indicates the low degree of crystallization of the products. Comparing the two XRD patterns, the peaks' intensity of Ni–Co oxide nanocomposite is dramatically lower than that of pure NiO. It indicates that the introduction of cobalt oxide can reduce the degree of crystallization of NiO. Energy dispersive spectrum (EDS) was also performed to ascertain the elemental composition in the formed sample C, shown as Fig. 1c. It can be seen that the as-synthesized material composed of Ni, Co, and O (the Au peak is attributed to measure base).

Analysis of microstructure and morphology

The surface morphology of products was determined by scanning electron microscope. Typical SEM image of sample A (n_{Co}=0) is shown in Fig. 2a. As seen in the Fig. 2a, pure NiO exhibits compact floc structure, which composed of fine nanoparticles agglomerate together. Figure 2b shows the representative SEM image of the

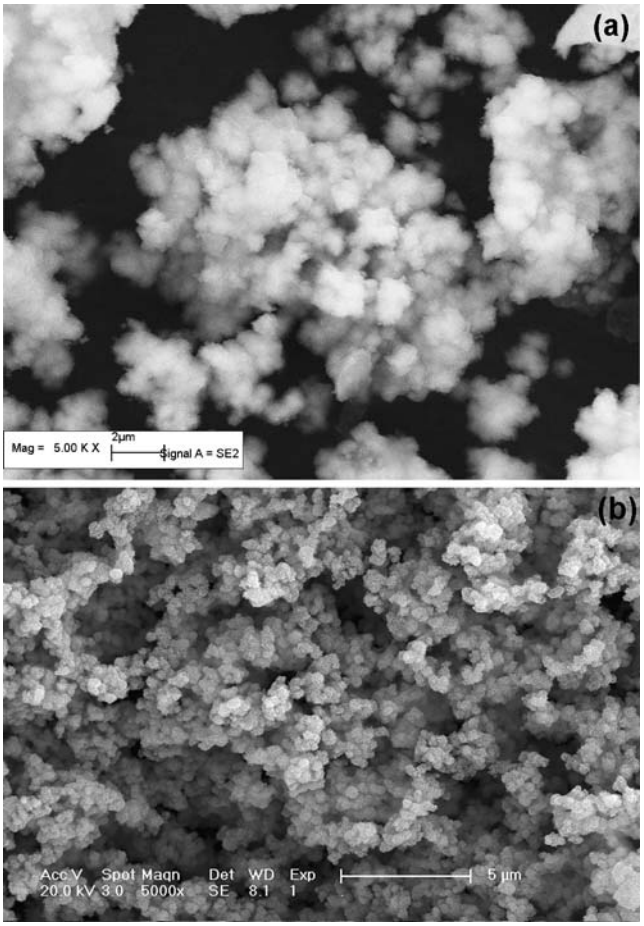

Fig. 2 SEM images of **a** sample A (n_{Co}=0) and **b** sample C (n_{Co}=0.5)

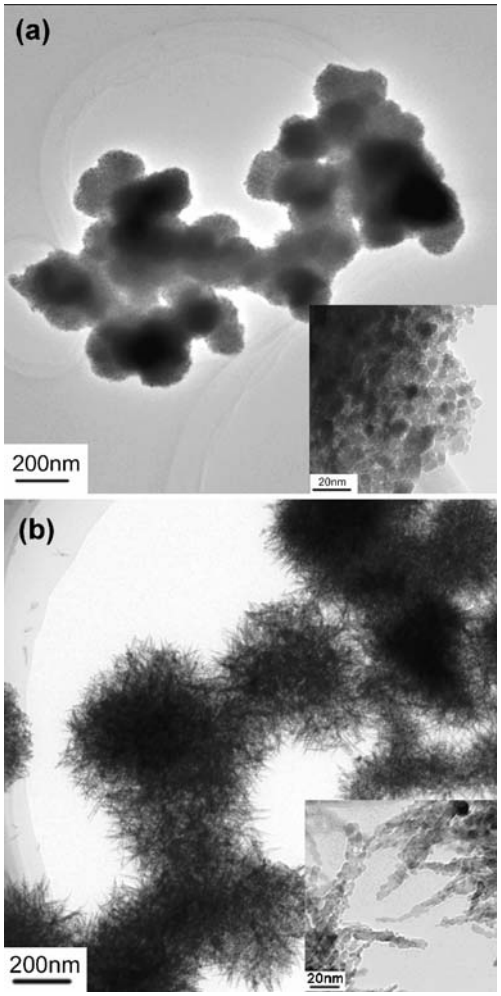

Fig. 3 TEM images of **a** sample A (n_{Co}=0) and **b** sample C (n_{Co}=0.5)

Ni–Co oxide composite with n_{Co}=0.5 (sample C). It can be seen that overgrowth of spherical clusters with a porous structure is clearly seen. Such surface morphology may offer increased surface area, more feasible for supercapacitor application.

Further characterization studies were carried out using TEM. The morphology of sample A (pure NiO) can be clearly seen in Fig. 3a. It composed of nanoparticles around 200 nm; further magnified can find that the nanoparticles are actually agglomerated by nanospheres with size about 8 nm (shown in insert). From Fig. 3b, one can see that the micrograph of sample C reveals an interesting structure of flocky spheroid. Careful observation can find that the flocky spheroid nanostructure is very loose and consists of numerous uniform nanowires. The inset in Fig. 3b shows the magnified image of the nanowires on the edge. The diameter of the nanowires is about 10–15 nm and length up to 100 nm. Comparing these two images, it can be found that after adding cobalt element, the microstructure of NiO changes from nanospheres to nanowires. It is known that the radii of Ni^{2+} ion is 0.070 nm and that of Co^{2+} ion is 0.072 nm. Both ions radii are close and easily form solid eutectic. We assume that the NiO and Co_3O_4 nanoparticles grow along certain direction and hence form the nanowires. This overgrowth can be explained on the basis of nucleation and coalescence process [18]. Initially grown

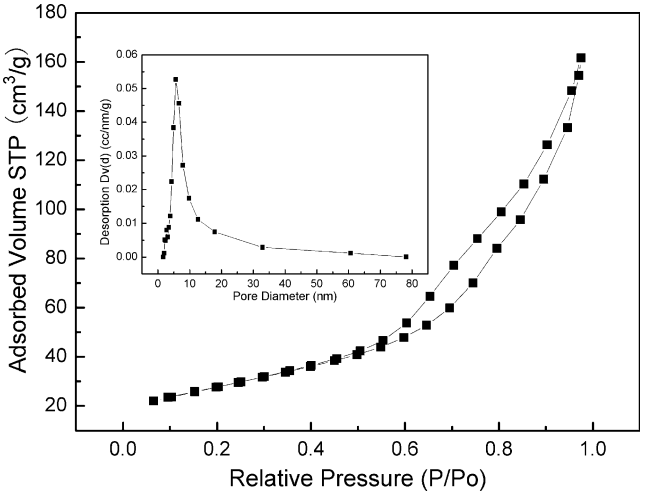

Fig. 4 The N_2 adsorption–desorption isotherm and pore size distribution of sample C (n_{Co}=0.5)

Table 1 Surface properties of sample A (n_{Co}=0) and C (n_{Co}=0.5), respectively

Sample	BET ($m^2\ g^{-1}$)	Pore volume ($cm^3\ g^{-1}$)	Average pore diameter (nm)
Sample A	160.916	0.166	3.437
Sample C	192.176	0.421	5.676

nanograins may have increased their size by further deposition and come closer to each other.

Nitrogen adsorption–desorption isotherms

To further analyze the structure of Ni–Co oxide nanocomposite, the nitrogen adsorption–desorption isotherms were measured. Figure 4 shows adsorption–desorption isotherms of sample C, and the pore size distribution curves obtained from the adsorption branch. The N_2 adsorption–desorption isotherm shows a strong hysteresis loop, which is an adsorption–desorption characteristic of the porous materials. The BET surface areas, calculated from adsorption isotherms, show that the surface area of the Ni–Co oxide is 192 $m^2\ g^{-1}$. The pore size distribution shown in Fig. 4 as an insert suggests that the as-synthesized sample C possesses a narrow mesoporous distribution at around 5–6 nm. No surfactant or organic dispersant was added in this experiment; the mesoporous structure may be attributed to the coordination homogeneous precipitation process. The hydrolysis rate is well controlled by dissociation of the coordination compound, which contributes to the stable skeleton of the mesoporous Ni–Co oxide. A comparison on pore structure parameters of sample A and sample C are listed in Table 1. It can be seen that the BET surface area, pore volume, and average pore diameter all increase with the introduction of cobalt ions into the nickel oxide matrix.

Electrochemical tests

CV response is a valuable tool to characterize the performance of electrochemical capacitors. Typical CV curves shown in Fig. 5a–d represent the voltammetric responses of sample A, B, C, and D, respectively. The shape of the curves reveals that the capacitance characteristic of Ni–Co oxide nanocomposite is distinct from that of the electric double-layer capacitor, which would produce a CV curve close to an ideal rectangular shape. A pair of broad redox

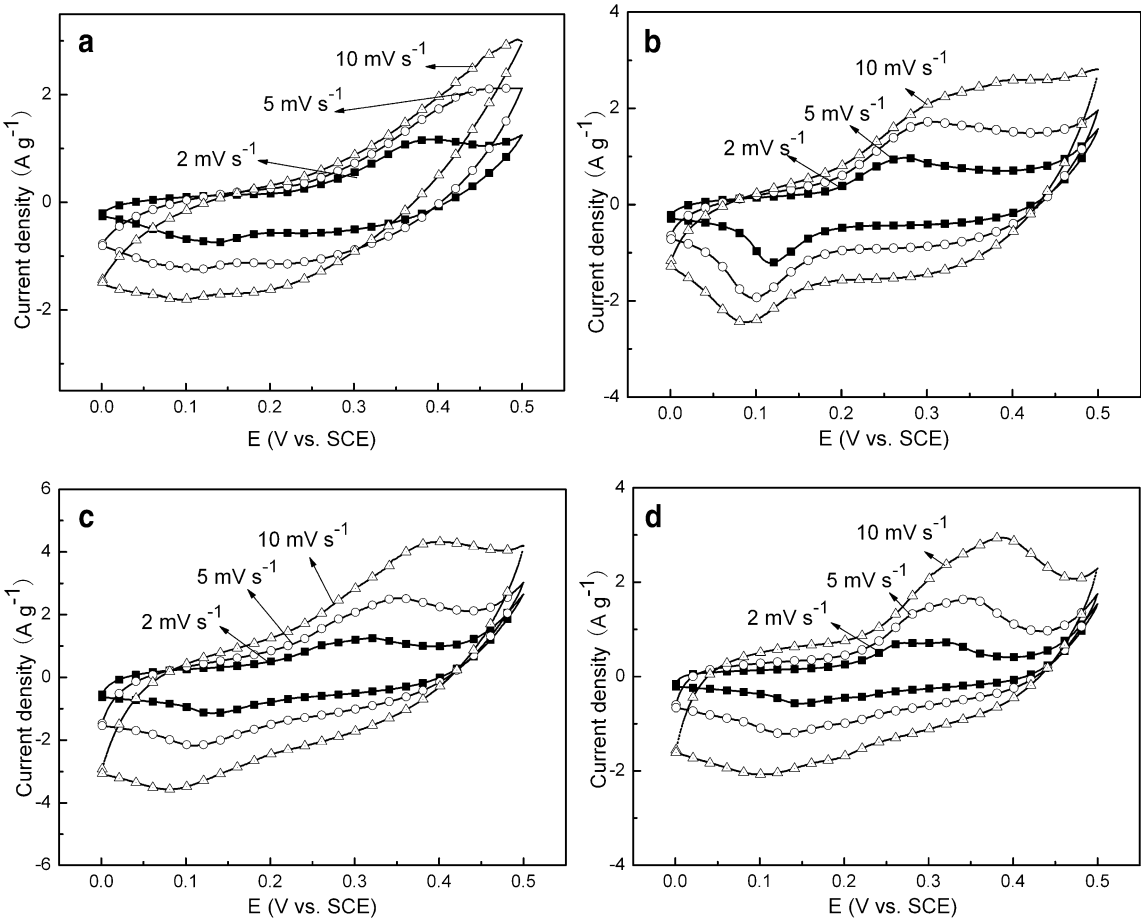

Fig. 5 CVs of samples A (**a**), B (**b**), C (**c**), and D (**d**) at different scan rates

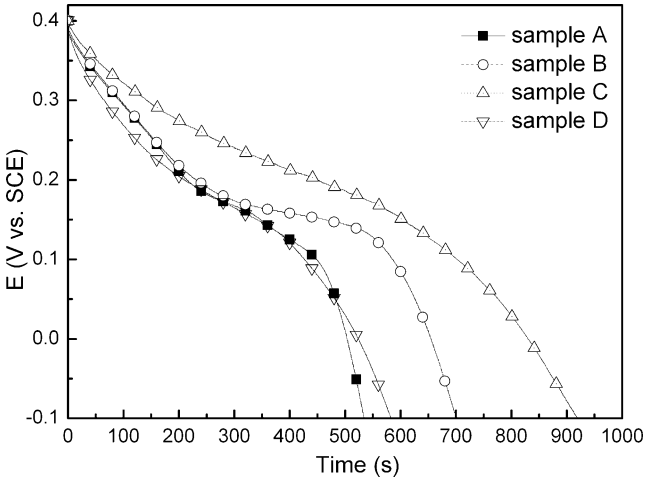

Fig. 6 The discharge curves of all samples at 0.2 A g^{-1}

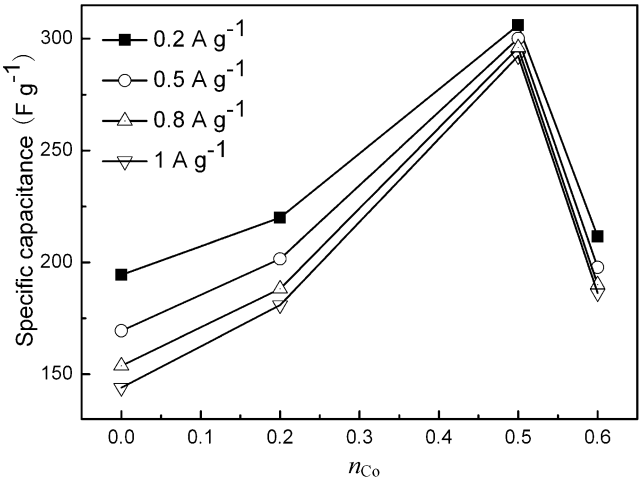

Fig. 7 Effect of amount of Co on specific capacitance of the composite material

peaks can be seen in these curves, indicating that the measured capacitance is mainly based on redox mechanism. Both the phases of NiO and Co_3O_4 in the composite are responsible for the pseudocapacitance. The pseudocapacitance reaction of NiO and Co_3O_4 in alkaline solution has been proposed as follows [8, 19]:

$$NiO + OH^- \underset{\text{discharge}}{\overset{\text{charge}}{\rightleftharpoons}} NiOOH + e^- \quad (1)$$

$$Co_3O_4 + H_2O + OH^- \underset{\text{discharge}}{\overset{\text{charge}}{\rightleftharpoons}} 3CoOOH + e^- \quad (2)$$

Note that the curve is more symmetric at low scan rate, as the scan rate increases, the profiles become gradually distort. This may be caused by an effective ions transport into the pores of active materials and small concentration polarization at the low scan rate; while at a higher scan rate, some active surface areas are inaccessible for charge storage [20] and big concentration polarization easily appeared. It is visible that the voltammetric current response in Fig. 5c is larger than that of other curves, which means that the specific capacitance of sample C is higher.

The specific capacitance (SC) values were evaluated from galvanostatic charge–discharge measurements, which are considered to be the most reliable. Figure 6 shows the discharge profiles of sample A, B, C, and D at 0.2 A g^{-1}, respectively. The corresponding SC values can be calculated by the following relationship [21, 22]:

$$C_m = \frac{I \times \Delta t}{\Delta V \times m} \quad (3)$$

where I is the current of charge/discharge, Δt is the time of discharge, ΔV is the potential range (in this paper, ΔV=0.5 V), and m is the mass of active materials. Compared these curves, sample C displays the longest discharge time, and the curve is nearly linear, indicating that sample C has better capacitive properties. This result is consistent with that of CV tests. The SC value of sample A, B, C, and D is calculated to be 194, 220, 306, and 211 F g^{-1}, respectively. The effect of amount of Co on specific capacitance of the composite material is shown in Fig. 7. From the curves in Fig. 7, one can see specific capacitance increases with increasing amount of Co from n_{Co}=0 to n_{Co}=0.5. On the contrary, specific capacitance decreases with increasing amount of Co from n_{Co}=0.5 to n_{Co}=0.6. Therefore, the specific capacitance can be affected by the amounts of Co in the composite material, optimum amount of Co is n_{Co}=0.5, and sample C with the amount of Co n_{Co}= 0.5 provides 306 F g^{-1} specific capacitance, which is 1.5 times greater than that of pure NiO. The enhanced capacitance may

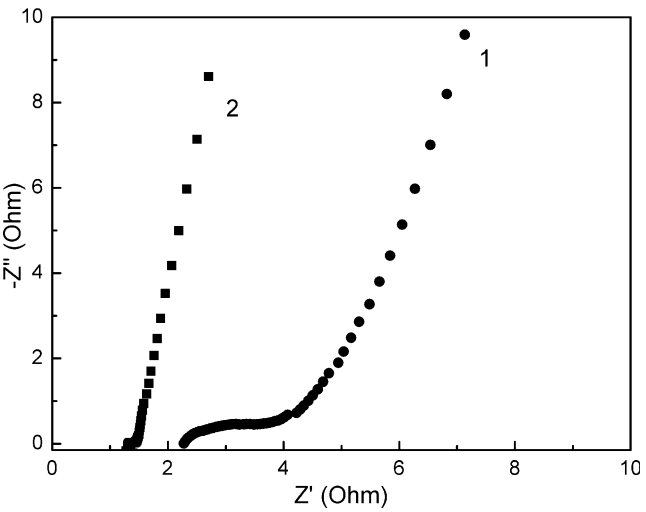

Fig. 8 The ac impedance plots of sample A (n_{Co}=0) and sample C (n_{Co}=0.5)

be considered for that the flocky structure of the composite makes it have bigger pore size and larger specific surface area (shown in Table 1), and the electrolyte easily soaks into the inner surface of material, which leads to a larger double layer capacitance. But it cannot solely explain the whole capacitance of the electrode. Compared sample C and A, the increase of BET surface area is just about 32 $m^2\ g^{-1}$, and this does not have much influence on values of capacity. So it is believed that the main part of the capacitance comes from the pseudocapacitive surface redox process. It is assumed that cobalt oxide inserted in nickel oxide system may lead to a distortion of the host lattice and induce defects in the structure and lead to an increase of redox active sites, so that composite materials possess higher charge storage capability.

The SC values for each sample at various discharge current densities are also shown in Fig. 7. In general, the specific capacitance decreases gradually with increasing discharge current density due to large IR drop at a large discharge current density that leads to the small specific capacitance [23]. As seen in Fig. 7, when the discharge current density increases from 0.2 to 1 A g^{-1}, SC value of sample C reduces about 4.5%, while the counterpart of sample A (pure NiO) is 29.5%, which is caused by the severe IR drop of the resistive electrodes. This indicates that Ni–Co oxide composite electrode has better charge–discharge properties at high current density than pure NiO electrode. This difference originates from the internal resistance of electrodes. It is possible that the introduction of Co can improve the electrode conductivity.

To further confirm the superiority of Ni–Co oxide nanocomposite than pure NiO, electrochemical impedance test was carried out at 0.5 V (vs. SCE) with a frequency range of 10^5 to 10^{-2} Hz on sample A and C. Figure 8 shows the corresponding impedance spectra as curve 1 (sample A) and 2 (sample C), respectively. The phase angles for impedance plots of both electrodes are observed to be higher than 45° in the low frequencies clearly. This result suggests that both electrodes are not controlled by diffusion process. At the high frequencies, half circle of sample C (curve 2) is smaller than that of sample A (curve 1) electrode, which indicates that its charge transition resistance is smaller. From the value of the point of intersecting with the real axis in the high frequency range, the internal resistances of sample C is about 1.3 Ω while the counterpart of sample A is about 2.2 Ω. Apparently, lower resistance is beneficial for the application of supercapacitors.

All in all, the mesoporous structure favors easy transfer of OH^- to the surface of active materials, and the addition of cobalt oxide into nickel oxide improves electrochemical activity. Therefore, the effective specific surface of material increases and the inner resistance of electrode decreases and its capacitance performance improves.

Conclusions

Mesoporous Ni–Co oxide nanocomposite has been synthesized by coordination homogeneous coprecipitation method. This method is simple, no need of washing process, and easy to realize the scale production. SEM and TEM results show that after the addition of cobalt element, the microstructure of NiO changes from nanospheres to nanowires which aggregate to form clusters with a porous structure. The specific capacitance of Ni–Co oxide nanocomposite with $n_{Co}=0.5$ is approximately 306 F g^{-1} in a 6-mol L^{-1} KOH electrolyte, which is 1.5 times greater than that of pure NiO electrode. The enhanced capacitance is attributed to that the flocky structure of Ni–Co oxide provides a larger effective surface area to produce nonfaradaic double-layer capacitance as well as a pseudocapacitance of faradaic redox on the particle surface. Additionally, the composite electrode also shows lower resistance and better charge–discharge properties at high current density. The as-prepared Ni–Co oxide composite may have promising applications in supercapacitors.

References

1. Prasad KR, Miura N (2004) Electrochem Commun 6:1004 doi:10.1016/j.elecom.2004.07.017
2. Xu MW, Zhao DD, Bao SJ, Li HL (2007) J Solid State Electrochem 11:1101 doi:10.1007/s10008-006-0246-4
3. Nathan T, Aziz A, Noor AF, Prabaharan SRS (2008) J Solid State Electrochem 12:1003 doi:10.1007/s10008-007-0465-3
4. Nam KW, Kim KH, Lee ES, Yoon WS, Yang XQ, Kim KB (2008) J Power Sources 182:642 doi:10.1016/j.jpowsour.2008.03.090
5. Zheng JP, Cygan PJ, Jow TR (1995) J Electrochem Soc 142:2699 doi:10.1149/1.2050077
6. Liu KC, Anderson MA (1996) J Electrochem Soc 143(1):124 doi:10.1149/1.1836396
7. Cheng J, Cao GP, Yang YS (2006) J Power Sources 159(1):734 doi:10.1016/j.jpowsour.2005.07.095
8. Nam KW, Kim K (2002) J Electrochem Soc 149(3):346 doi:10.1149/1.1449951
9. Srinivasan V, Weidner JW (1997) J Electrochem Soc 144(8):210 doi:10.1149/1.1837859
10. Zhang FB, Zhou YK, Li HL (2004) Mater Chem Phys 83:260 doi:10.1016/j.matchemphys.2003.09.046
11. Xu MW, Bao SJ, Li HL (2007) J Solid State Electrochem 11:372 doi:10.1007/s10008-006-0155-6
12. Wu MQ, Gao JH, Zhang SR, Chen A (2006) J Power Sources 159:365 doi:10.1016/j.jpowsour.2006.04.013
13. Liang K, Chen A, He L, Wang W (2002) J Mar Sci Technol 18 (4):383 doi:10.1179/026708302225001642
14. Watanabe KI, Koseki M, Kumagai N (1996) J Power Sources 58:23 doi:10.1016/0378-7753(95)02272-4
15. Wang XY, Yan J, Yuan HT, Zhang YS, Song DY (1999) Int J Hydrogen Energy 24:973 doi:10.1016/S0360-3199(98)00130-X
16. Chang JK, Shong DS, Tsai WT (2002) J Power Sources 103:280 doi:10.1016/S0378-7753(01)00866-7
17. Hu CC, Cheng CY (2002) Electrochem Solid-State Lett 5(3):43 doi:10.1149/1.1448184

18. Shinde VR, Mahadik SB, Gujar TP, Lokhande CD (2006) Appl Surf Sci 252:7487 doi:10.1016/j.apsusc.2005.09.004
19. Srinivasan V, Weidner JW (2002) J Power Sources 108:15 doi:10.1016/S0378-7753(01)01012-6
20. Huang QH, Wang XY, Li J, Dai CL, Gamboa S, Sebastian PJ (2007) J Power Sources 164:425 doi:10.1016/j.jpowsour.2006.09.066
21. He KX, Wu QF, Zhang XG, Wang XL (2006) J Electrochem Soc 153(8):1568 doi:10.1149/1.2208735
22. Tao F, Shen YZ, Liang YY, Li HL (2007) J Solid State Electrochem 11:853 doi:10.1007/s10008-006-0232-x
23. Lee JY, Liang K, An KH, Lee YH (2005) Synth Met 150:153 doi:10.1016/j.synthmet.2005.01.016